

Article

# Study on Ultra-High Temperature Contact Solution Treatment of Al–Zn–Mg–Cu Alloys

Wenming Jin <sup>1,2</sup>, Jianhao Yu <sup>1</sup>, Zhiqiang Zhang <sup>1,\*</sup>, Hongjie Jia <sup>1,3</sup> and Mingwen Ren <sup>1,3</sup>

<sup>1</sup> Key Laboratory of Automobile Materials, Ministry of Education, and College of Material Science and Engineering, Jilin University, Changchun 130025, China; jwmjlu@126.com (W.J.); yjhjlu@126.com (J.Y.); jiahj@jlu.edu.cn (H.J.); renmw@jlu.edu.cn (M.R.)

<sup>2</sup> Roll Forging Research Institute, Jilin University, Changchun 130025, China

<sup>3</sup> Superplastic and Plastic Institute, Jilin University, Changchun 130025, China

\* Correspondence: zhangzq@jlu.edu.cn; Tel.: +86-431-85094376

**Abstract:** Contact solution treatment (CST) of Al–Zn–Mg–Cu alloys can shorten solution time to within 40 s in comparison with 1800 s with traditional solution treatment using a heating furnace. Heating temperature is the key factor in solution treatment. Considering the short heating time of CST, the ultra-high solution temperature over 500 °C of Al–Zn–Mg–Cu alloys was studied in this work. The effects of solution temperatures on the microstructures and the mechanical properties were investigated. The evolution of the second phases was explored and the strengthening mechanisms were also quantitatively evaluated. The results showed that solution time could be reduced to 10 s with the solution temperature of 535 °C due to the increasing dissolution rate of the second phase and the tensile strength of the aged specimen could reach 545 MPa. Precipitation strengthening was the main strengthening mechanism, accounting for 75.4% of the total strength. Over-burning of grain boundaries occurred when the solution temperature increased to 555 °C, leading to the deterioration of the strength.

**Keywords:** Al–Zn–Mg–Cu alloys; contact solution treatment; microstructures; mechanical properties; strengthening mechanism



**Citation:** Jin, W.; Yu, J.; Zhang, Z.; Jia, H.; Ren, M. Study on Ultra-High Temperature Contact Solution Treatment of Al–Zn–Mg–Cu Alloys. *Metals* **2021**, *11*, 842. <https://doi.org/10.3390/met11050842>

Received: 27 April 2021

Accepted: 18 May 2021

Published: 20 May 2021

**Publisher's Note:** MDPI stays neutral with regard to jurisdictional claims in published maps and institutional affiliations.



**Copyright:** © 2021 by the authors. Licensee MDPI, Basel, Switzerland. This article is an open access article distributed under the terms and conditions of the Creative Commons Attribution (CC BY) license (<https://creativecommons.org/licenses/by/4.0/>).

## 1. Introduction

Hot stamping (HS) of Al alloys is increasingly applied to the manufacture of automotive body parts due to the demand for vehicle weight reduction. In HS, solution treatment is needed firstly to make the second phases fully dissolve in the Al matrix and then the hot blank is transferred to the cold die for in-die forming and quenching, followed by T6 ageing treatment to obtain high-strength formed parts [1,2]. The solution treatment of Al alloys is generally conducted by heating furnaces. The HS experiment of a B pillar made of 7075 Al alloys conducted by Harrison et al. [3] showed that the solution time is 1800 s and the forming and quenching time is only 20 s, which indicates that too long a solution time cannot be synchronized with subsequent forming and quenching processes. Exploring new solution treatment methods and shorten solution time is highly significant for the manufacturing of Al alloy HS parts. Although the pulse current and the salt bath furnace solution treatment put forward by Xu et al. [4,5] and Chang et al. [6] can shorten solution time to some degree, the factors, such as current stability and salt bath duration, limit the application of these methods. Zhang et al. [7,8] have found that contact solution treatment (CST) can significantly shorten the solution time within 40 s and the mechanical properties of the specimens after ageing are slightly better than those of the solution treatment specimens by a heating furnace.

Solution temperature is generally determined by dissolving temperature of soluble phase. The temperature of 475 °C is currently regarded as the solution temperature of Al–Zn–Mg–Cu alloys [9], but some studies have shown that the second phases cannot be

fully dissolved at 475 °C. Mazibuko and Curle [10] have confirmed that Al<sub>2</sub>CuMg phase can fully dissolve into the Al matrix with the solution temperature of 490 °C. However, the high solution temperature and the long solution time in a heating furnace will lead to grain growth and insoluble phase coarsening, which will have a negative impact on material properties. There are currently very few studies that explore ultra-high temperature (higher than 475 °C) solution treatment of Al–Zn–Mg–Cu alloys.

Considering the high heat rate and the short heating time of CST, the CST experiments of Al–Zn–Mg–Cu alloys with solution temperature over 500 °C were conducted and the effect of the solution temperatures on the microstructures and the mechanical properties of Al–Zn–Mg–Cu alloys was investigated in this study.

## 2. Materials and Methods

The 2 mm 7075-T6 Al alloy was used and its chemical composition is shown in Table 1. The experimental device is shown in Figure 1. It mainly consists of the upper contact body, lower contact body, and cartridge heaters. The specimens were put between two heated contact bodies to be heated with different holding time (including heating time). For the detailed contact solution device and methods refer to references [7,8]. Three solution temperatures were used to study the effect of solution temperature on the microstructures and the mechanical properties. The experimental parameters are shown in Table 2. Three specimens were repeated for each condition. After being quenched, artificial aging (AA) treatment of solution specimens was conducted at 120 °C for 24 h. Figure 2 displays the heating rates with different solution temperatures. When the contact bodies temperature is 475 °C, the heating rate of the specimen is 15.8 °C/s and the temperature of the specimen can reach 470 °C with 30 s holding time. With the contact bodies temperature increasing to 535 °C, the heating rate rises to 50 °C/s and the temperature of the specimen can reach 500 °C within 10 s. When the contact bodies temperature is increased to 555 °C, the heating rate of the specimen changes little, and the temperature of the specimen reaches 515 °C after holding for 10 s.

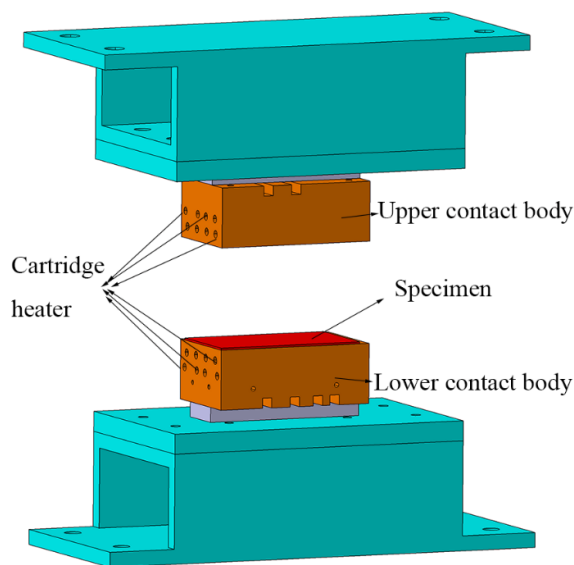


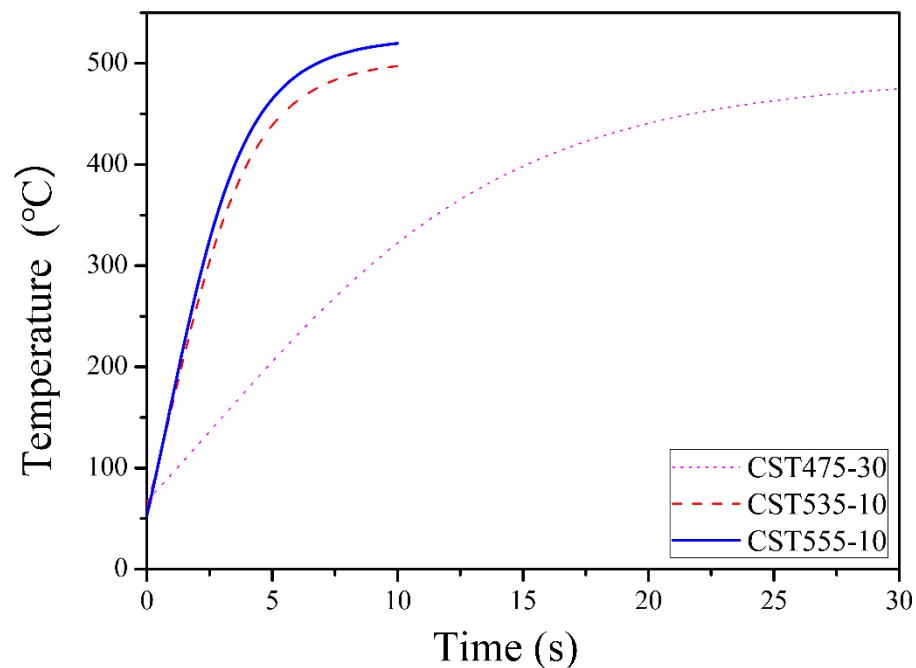
Figure 1. Experimental device.

Table 1. Chemical composition of 7075 Al alloy (wt%).

Element	Zn	Mg	Cu	Fe	Si	Mn	Cr	Ti	Other	Al
wt%	5.1~ 6.1	2.1~ 2.9	1.2~ 2.0	≤0.5	≤0.4	≤0.3	≤0.2	≤0.2	0.15	Bal

**Table 2.** Experimental parameters of contact solution treatment (CST).

Conditions	Contact Body Temperature/ $^{\circ}\text{C}$	Holding Time/s	Holding Pressure/MPa	Temperature of the Specimen/ $^{\circ}\text{C}$
CST475-40	475	30	20	470
CST535-10	535	10	20	500
CST555-10	555	10	20	515

**Figure 2.** Temperature variation curves of specimens with different CSTs.

Uniaxial tensile tests were conducted using a universal testing machine (WDW-300) at room temperature with an initial strain rate of  $1 \times 10^{-3} \cdot \text{s}^{-1}$ . The specimens with the gauge section of  $30 \text{ mm} \times 4 \text{ mm}$  was used in this study. Each condition was repeated for three times. The electrical conductivity of the quenched specimens was measured using the Sigma2008 eddy current meter.

Keller reagents (1 mL HF, 1.5 mL HCL, 2.5 mL HNO<sub>3</sub> and 95 mL H<sub>2</sub>O) were used to etch the microscopic specimens. The morphology and grain size of the specimens were observed using a ZEISS optical microscope (OM). The second phases of quenched specimens were measured using a D/max-2500PC X-ray diffractometer. Transmission electron microscope (TEM) specimens were made by ion polishing and then were examined with a JEM-2100 TEM operated at 200 kV.

### 3. Results and Discussion

#### 3.1. Analysis of Mechanical Properties

The engineering stress vs. strain curves for the specimens after ageing treatment are shown in Figure 3. The yield strength, tensile strength and elongation of the specimens are presented in Table 3. Compared with the CST475-30 + AA specimen, the strength of the CST535-10 + AA specimen increases slightly and the tensile strength reaches 545 MPa. This may be due to the fact that the high solution temperature in CST can accelerate the dissolution of the second phases. However, the strength of the CST555-10 + AA specimen decrease dramatically, which may be the result of the second phases coarsening. The decrease of elongation may be caused by the over-burning of grain boundaries due to temperature being too high.

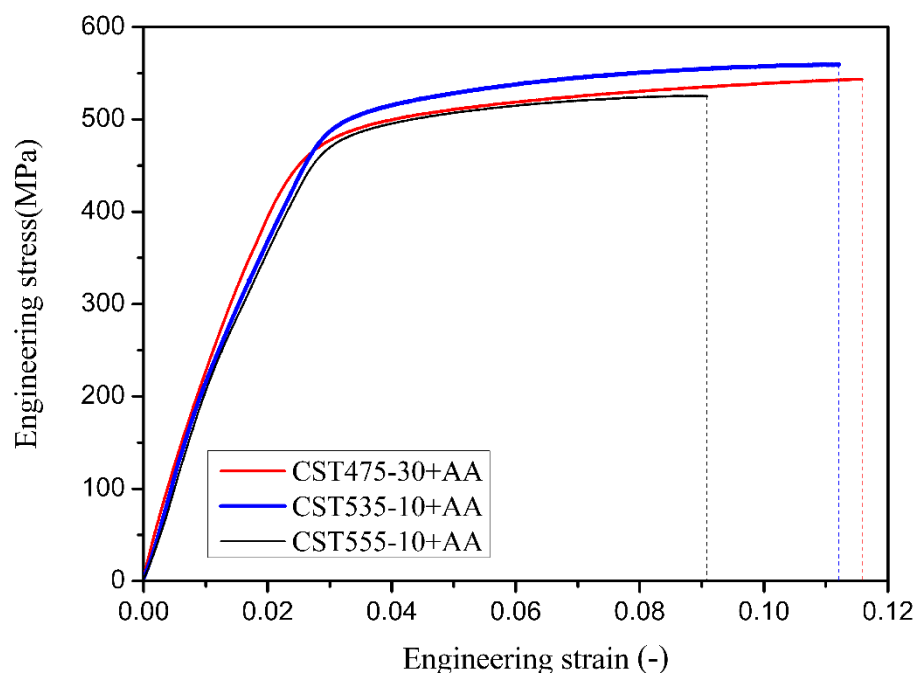


**Figure 3.** Engineering stress vs. strain curves at different solution temperatures.

**Table 3.** Yield strength, tensile strength and elongation of the specimens after ageing treatment with different solution temperatures.

Conditions	Yield Strength (MPa)	Tensile Strength (MPa)	Elongation (%)
CST475-30 + AA	465	538	11.6
CST535-10 + AA	472	545	11.2
CST555-10 + AA	418	523	9.1

### 3.2. Grain Morphology Observation

Figure 4 displays the optical microstructures of the quenched specimens with different solution temperatures. The CST475-30 and CST535-10 specimens exhibit even grains distribution, as shown in Figure 4a,b. Grain size was measured using Image J software and the results are shown in Figure 4d,e. The average grain sizes of the CST475-30 and CST535-10 specimens are  $45 \pm 5.4 \mu\text{m}$  and  $41 \pm 7.3 \mu\text{m}$ , respectively. There is little difference in grain size between them. The grain boundaries of the CST555-10 specimen show obvious coarsening (refer to Figure 4c) because of the local over-burning, which is the main reason for the decrease in the mechanical properties. Therefore, the solid temperature of 555 °C has a significant negative impact on the mechanical properties.

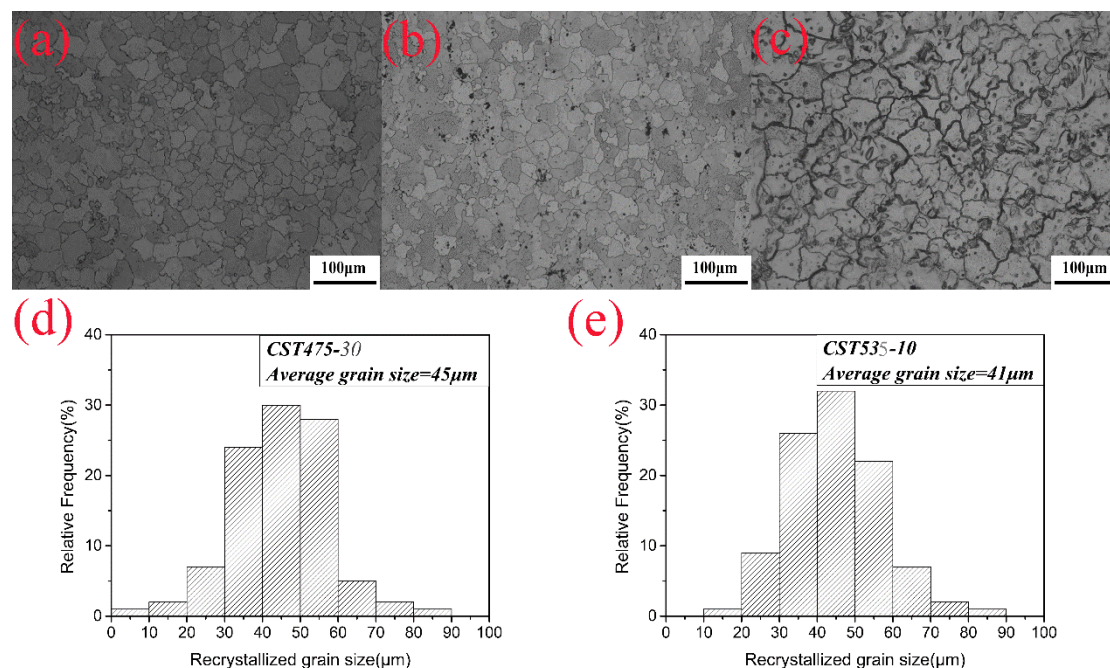


**Figure 4.** Optical microstructures of quenched specimens (a) CST475-30 (b) CST535-10 (c) CST555-10 (d) CST475-30 grain size distribution (e) CST535-10 grain size distribution.

Because the original material had been treated with T6 condition, the initial deformation energy storage is small, so it can be considered that there is no work hardening. Due to the short solution time, the grains hardly grow and coarsen [11,12]. The grain boundary strengthening effects of the CST475-30 and CST535-10 specimens were quantified using the Hall–Petch equation:

$$\Delta\sigma = \sigma_y - \sigma_0 = \frac{k_y}{\sqrt{d}} \quad (1)$$

where  $d$  is average grain diameter,  $\sigma_0$  is friction stress and  $k_y$  is Hall–Petch coefficient. Wert et al. [13–15] have investigated the effect of grain size on the yield strength of the 7000 series Al alloys, and have obtained the Hall–Petch coefficient  $k_y$  of 7075 Al alloy is 0.12 MPa/m [16,17]. The grain boundary strengthening contributions of the CST475-30 and CST535-10 specimens are 17.89 MPa and 18.74 MPa, respectively. There is a difference of 0.85 MPa and the proportion of strengthening contribution under these two conditions does not exceed 4%.

### 3.3. Analysis of the Second Phases Evolution

Figure 5 shows the X-ray diffraction (XRD) results of the CST475-30 and CST535-10 specimens. The second phases of Al–Zn–Mg–Cu alloys are mainly composed of the low-melting  $\text{MgZn}_2$  phase, the high-melting  $\text{Al}_2\text{CuMg}$  phase, and the insoluble phases such as  $\text{Mg}_2\text{Si}$  and  $\text{Al}_7\text{Cu}_2\text{Fe}$  [18,19]. After solution treatment, the phase peaks of  $\text{MgZn}_2$  and  $\text{Al}_2\text{CuMg}$  basically disappear, which indicates that most of  $\text{MgZn}_2$  and  $\text{Al}_2\text{CuMg}$  phases dissolve. Using the calculation, the lattice parameters  $a$  of the two specimens are 4.0627 nm and 4.0638 nm, respectively. It can be inferred that the lattice distortion of CST535-10 specimen is larger because of more second-phase dissolution. The second phase solubility is inversely proportional to the conductivity [20]. The conductivities of the quenched CST475-30 and CST535-10 specimens are 18.2 MS/m and 17.8 MS/m, respectively. It can also demonstrate that the lattice distortion of the CST535-10 specimen is larger, which is in agreement with the results of the lattice parameters calculation.

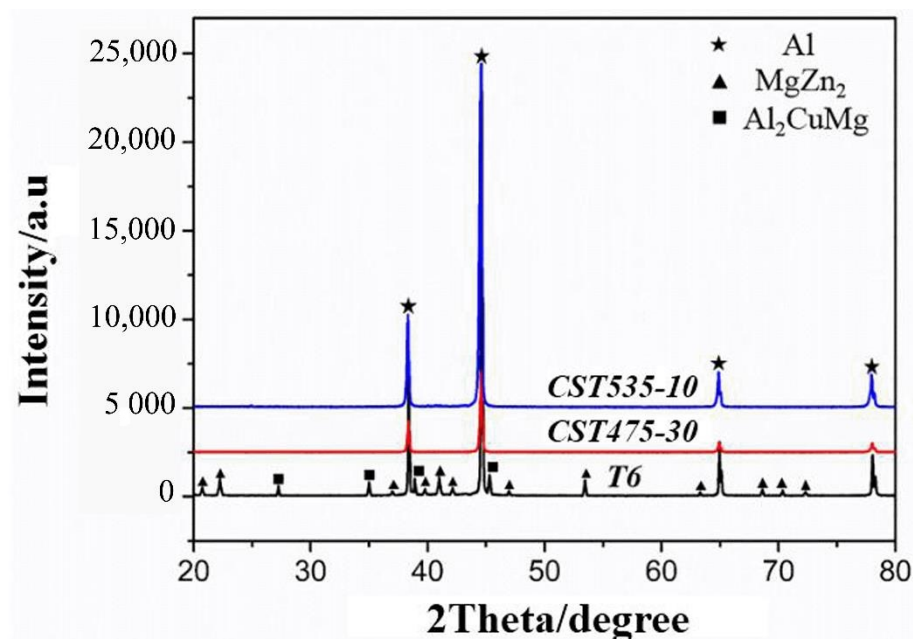


Figure 5. X-ray diffraction (XRD) with different solution temperatures.

For the CST, the increase of the contact bodies temperature resulted in the increase of temperature difference between the contact bodies and the specimen and thus the heat input per unit time was increased. High heating rate can increase the equilibrium temperature of phase transformation, which shortens the dissolution time of GP regions and low-melting  $MgZn_2$  phase.

The dissolution rate of the high-melting eutectic phases is mainly determined by thermodynamic equilibrium temperatures. Because the heating rate is limited in the solution treatment by using the heating furnace, the eutectic phases with different melting temperatures dissolve into the matrix in a certain sequence, which results in the long dissolution time [21,22]. The melting point of the  $Al_2CuMg$  phase is about  $450\text{ }^\circ\text{C}$ , and the CST475-30 specimen needs 20 s to reach  $450\text{ }^\circ\text{C}$ . Due to thermal lag effect, it is generally believed that the dissolution temperature of the  $Al_2CuMg$  phase is about  $15\text{ }^\circ\text{C}$  lower than the specimen temperature [23]. Therefore, it is impossible to dissolve the  $Al_2CuMg$  phase in a short time at traditional optimal solution temperature of  $475\text{ }^\circ\text{C}$ . Additionally, Wen et al. [24] believed that the solute atoms such as Zn, Mg, Cu etc. will regenerate  $Al_2CuMg$  phase in the local regions with solution temperature below  $450\text{ }^\circ\text{C}$  due to their different diffusion rates in solution treatment. Peng et al. [25,26] found that  $Al_2CuMg$  phase will hardly dissolve and even coarsen with the temperature below  $450\text{ }^\circ\text{C}$ , which will have a significant negative impact on the dissolution process. Moreover, Liu et al. [27] have studied the dissolution of the  $Al_2CuMg$  phase and found that the full dissolution temperature needs to be  $493\text{ }^\circ\text{C}$ . Deng et al. [28] have designed two-stage solution treatment for Al–Zn–Mg–Cu alloys and used the temperature over  $490\text{ }^\circ\text{C}$  in the second stage, aimed at making the  $Al_2CuMg$  phase fully dissolve. In the CST with ultra-high temperature, the temperature of the CST535-10 specimen could increase to more than  $450\text{ }^\circ\text{C}$  in 5 s, and reached  $500\text{ }^\circ\text{C}$  with 10 s. Therefore, there was no aggregation of  $Al_2CuMg$  phase during rapid dissolution process.

The dissolution of soluble phases in ultra-high temperature CST mainly occurred in the high-temperature range. The solute atoms moved faster due to the high temperature and large diffusion coefficient, while the elastic stress field in the aluminum matrix decreased or even disappeared under the influence of high temperature, which was conducive to the diffusion of solute atoms in the aluminum matrix.

The increase of solution time may result in coarsening of insoluble phase. In the process of solid solution, Cu atoms will gather around Fe-rich phase (such as  $AlFe_3$  phase)

by the driving force of high temperature and make it most likely transform into a more stable  $\text{Al}_7\text{Cu}_2\text{Fe}$  phase. The research results of Zou et al. [29] also showed that long solution time will cause the coarsening of the  $\text{Mg}_2\text{Si}$  phase. The coarsening of the insoluble phases such as  $\text{Al}_7\text{Cu}_2\text{Fe}$  and  $\text{Mg}_2\text{Si}$  will consume solute elements during the ageing process and reduce the strength of the alloy [30–32]. Therefore, the short solution time of 10 s in the ultra-high temperature CST was beneficial to reduce the negative effect of the insoluble phases coarsening.

Figure 6 displays the TEM microstructures of the specimens after ageing treatment. Compared with the CST475-30 + AA specimen, the number densities of the precipitates of the CST535-10 + AA specimen were obviously increased. The reason is that the ultra-high solid solution temperature could eliminate the segregation of solute elements in the alloy, which was beneficial to the nucleation and precipitation of the second phases. In addition, the solution temperature increase would obtain the higher supersaturated vacancy concentration after quenching and promote the dispersed precipitation and uniform distribution of the second phases. Therefore, the precipitation strengthening effect of the CST535-10 + AA specimen was better. For Al–Zn–Mg–Cu alloys, Orowan strengthening is the main strengthening mechanism, and the strengthening effect mainly depends on the size and quantity of the second phase particles, as shown in Equation (2):

$$\Delta\sigma_{\text{orowan}} = M \frac{0.4Gb}{\pi\sqrt{1-\nu}} \frac{\ln(2\bar{r}/b)}{\lambda_p} \quad (2)$$

where  $b$  is the Burgers vector and  $b = 0.286 \mu\text{m}$ .  $M$  is average orientation factor, for the 7075 Al alloy with fcc structure,  $M = 3.06$ .  $G$  is shear modulus of 26.9 GPa.  $\nu$  is Poisson's ratio of 0.33.  $\bar{r}$  is calculated diameter of precipitates, generally  $\bar{r} = \sqrt{2/3}r$ ,  $r$  is average diameter of statistical measurement.  $\lambda_p$  is mean edge-to-edge interprecipitate spacing [33,34]. The average precipitates sizes of the CST475-30 + AA and CST535-10 + AA specimens are  $60 \pm 7.2 \text{ nm}$  and  $48 \pm 4.6 \text{ nm}$ , and the mean spacing are 56 nm and 50 nm, respectively. The precipitation strengthening contributions of the CST475-30 + AA and CST535-10 + AA specimens are 382 MPa and 411 MPa, respectively.

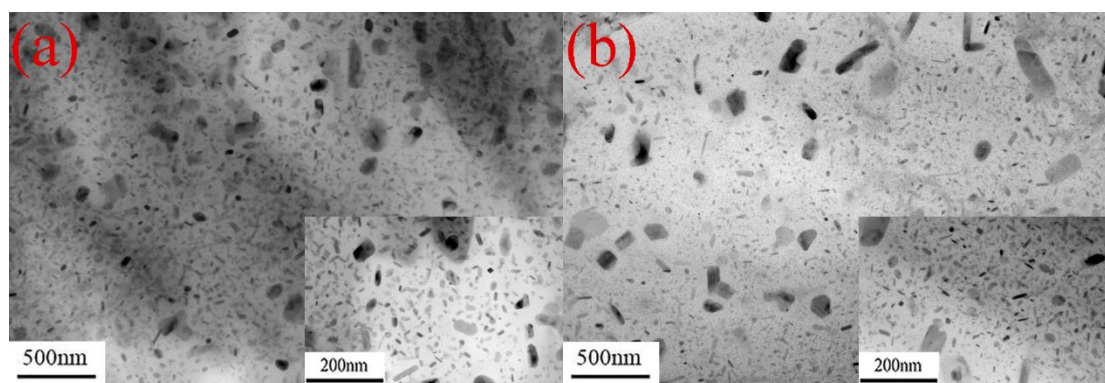


**Figure 6.** Transmission electron microscopy (TEM) micrograph of 7075 Al alloy after ageing treatment, (a) CST475-30 + AA, (b) CST535-10 + AA.

#### 4. Conclusions

This paper investigated the effect of ultra-high temperature CST on the microstructures and mechanical properties of 7075 Al alloy. The results are shown as follows:

- (1) With the increase of the solution temperature, the temperature rise rate of the specimen increased and the holding time decreased. When the solution temperatures were 475 °C and 535 °C, the mechanical properties of the specimens were similar. However, when the solution temperature increased to 555 °C, the grain boundaries of the

specimen showed local over-burning, leading to the decrease in the mechanical properties.

- (2) With the contact bodies' temperature of 535 °C and holding time of 10 s, the dissolution of low-melting MgZn<sub>2</sub> phase was fast and the coarsening of the high-melting Al<sub>2</sub>CuMg phase in the low-temperature range was avoided. The tensile strength of the specimen was 545 MPa after artificial aging, and the contribution of precipitation strengthening was 411 MPa, accounting for about 75.4% of the total strength.

**Author Contributions:** W.J. contributed to the conception of the study. J.Y. performed the experiment. Z.Z. performed the data analyses and wrote the manuscript. H.J. contributed significantly to analysis and manuscript preparation. M.R. helped perform the analysis with constructive discussions. All authors have read and agreed to the published version of the manuscript.

**Funding:** This research received no external funding.

**Institutional Review Board Statement:** Not applicable.

**Informed Consent Statement:** Not applicable.

**Data Availability Statement:** The data used to support the findings of this study are available from the corresponding author upon request.

**Conflicts of Interest:** The authors declare no conflict of interest.

## References

1. Wang, L.; Strangwood, M.; Balint, D.; Lin, J.; Dean, T.A. Formability and failure mechanisms of AA2024 under hot forming conditions. *Mater. Sci. Eng. A* **2011**, *528*, 2648–2656. [[CrossRef](#)]
2. Ko, D.C.; Ko, D.H.; Kim, J.H.; Park, J.H. Development of a partition panel of an Al6061 sheet metal part for the improvement of formability and mechanical properties by hot forming quenching. *Adv. Mech. Eng.* **2017**, *9*, 1–15. [[CrossRef](#)]
3. Harrison, N.R.; Luckey, S.G. Hot Stamping of a B-Pillar Outer from High Strength Aluminum Sheet AA7075. *SAE Int. J. Mater. Manuf.* **2014**, *7*, 567–573. [[CrossRef](#)]
4. Xu, X.; Zhao, Y.; Ma, B.; Zhang, J.; Zhang, M. Rapid grain refinement of 2024 Al alloy through recrystallization induced by electropulsing. *Mater. Sci. Eng. A* **2014**, *612*, 223–226. [[CrossRef](#)]
5. Xu, X.; Zhao, Y.; Wang, X.; Zhang, Y.; Ning, Y. Effect of rapid solid-solution induced by electropulsing on the microstructure and mechanical properties in 7075 Al alloy. *Mater. Sci. Eng. A* **2016**, *654*, 278–281. [[CrossRef](#)]
6. Chang, Y.L.; Huang, F.Y.; Lui, T.S. Enhancing the tensile yield strength of A6082 aluminum alloy with rapid heat solutionizing. *Mater. Sci. Eng. A* **2017**, *702*, 438–445. [[CrossRef](#)]
7. Zhang, Z.Q.; Yu, J.H.; He, D.Y. Influence of contact solid-solution treatment on microstructures and mechanical properties of 7075 aluminum alloy. *Mater. Sci. Eng. A* **2019**, *743*, 500–503. [[CrossRef](#)]
8. Zhang, Z.Q.; Yu, J.H.; He, D.Y. Effects of contact body temperature and holding time on the microstructure and mechanical properties of 7075 aluminum alloy in contact solid solution treatment. *J. Alloys Compd.* **2020**, *823*, 153919. [[CrossRef](#)]
9. Xu, D.K.; Rometsch, P.A.; Birbilis, N. Improved solution treatment for an as-rolled Al–Zn–Mg–Cu alloy. Part II. Characterisation of constituent particles and overheating. *Mater. Sci. Eng. A* **2012**, *534*, 234–243. [[CrossRef](#)]
10. Mazibuko, N.E.; Curie, U.A. Effect of solution heat treatment time on a rheocast Al-Zn-Mg-Cu Alloy. In *Materials Science Forum*; Trans Tech Publications Ltd.: Stafa-Zurich, Switzerland, 2011; Volume 690, pp. 343–346.
11. Ashrafizadeh, S.M.; Eivani, A.R.; Jafarian, H.R.; Zhou, J. Improvement of mechanical properties of AA6063 aluminum alloy after equal channel angular pressing by applying a two-stage solution treatment. *Mater. Sci. Eng. A* **2017**, *687*, 54–62. [[CrossRef](#)]
12. Fan, Y.Q.; Wen, K.; Li, Z.H.; Li, X.W.; Zhang, Y.A.; Xiong, B.Q.; Xie, J.X. Microstructure of as-extruded 7136 aluminum alloy and its evolution during solution treatment. *Rare Met.* **2017**, *36*, 256–262. [[CrossRef](#)]
13. He, Y.; Jia, Z.H.; Sanders, R.E.; Liu, Y.Y.; Ding, L.P.; Xing, Y.; Liu, Q. Quantitative study of dissolution of Mg<sub>2</sub>Si during solution treatment in AA6014 alloy. *J. Alloys Compd.* **2017**, *703*, 272–279. [[CrossRef](#)]
14. Pande, C.S.; Cooper, K.P. Nanomechanics of Hall–Petch relationship in nanocrystalline materials. *Prog. Mater. Sci.* **2009**, *54*, 689–706. [[CrossRef](#)]
15. Cao, B.; Joshi, S.P.; Ramesh, K.T. Strengthening mechanisms in cryomilled ultrafine-grained aluminum alloy at quasi-static and dynamic rates of loading. *Scr. Mater.* **2009**, *60*, 619–622. [[CrossRef](#)]
16. Lavernia, E.J.; Han, B.Q.; Schoenung, J.M. Cryomilled nanostructured materials: Processing and properties. *Mater. Sci. Eng. A* **2008**, *493*, 207–214. [[CrossRef](#)]
17. Witkin, D.B.; Lavernia, E.J. Synthesis and mechanical behavior of nanostructured materials via cryomilling. *Prog. Mater. Sci.* **2006**, *51*, 1–60. [[CrossRef](#)]
18. Cong, F.; Zhao, G.; Jiang, F.; Tian, N.; Li, R. Effect of homogenization treatment on microstructure and mechanical properties of DC cast 7X50 aluminum alloy. *Trans. Nonferrous Met. Soc. China* **2015**, *25*, 1027–1034. [[CrossRef](#)]

19. Rokhlin, L.L.; Dobatkina, T.V.; Bochvar, N.R.; Lysova, E.V. Investigation of phase equilibria in alloys of Al–Zn–Mg–Cu–Zr–Sc system. *J. Alloys Compd.* **2004**, *367*, 10–16. [[CrossRef](#)]
20. Chen, S.Y.; Chen, K.H.; Peng, G.S.; Peng, L.J.; Dong, X. Effect of heat treatment on strength, exfoliation corrosion and electrochemical behavior of 7085 aluminum alloy. *Mater. Des.* **2012**, *35*, 93–98. [[CrossRef](#)]
21. Bjørnekletta, B.I.; Gronga, Ø.; Myhrb, O.R.; Kluckenb, A.O. Additivity and isokinetic behaviour in relation to particle dissolution. *Acta Mater.* **1998**, *46*, 6257–6266. [[CrossRef](#)]
22. Todaa, H.; Nishimuraa, T.; Uesugib, K.; Suzukib, Y.; Kobayashia, M. Influence of high-temperature solution treatments on mechanical properties of an Al–Si–Cu aluminum alloy. *Acta Mater.* **2010**, *58*, 2014–2025. [[CrossRef](#)]
23. Djurdjevic, M.B.; Kierkus, C.A.; Northwood, D.O.; Sokolowski, J.H. Improvement of 319 aluminum alloy casting durability by high temperature solution treatment. *J. Mater. Process. Technol.* **2001**, *109*, 174–180.
24. Wen, K.; Xiong, B.Q.; Fan, Y.Q.; Zhang, Y.A.; Li, Z.H.; Li, X.W.; Wang, F.; Liu, H.W. Transformation and Dissolution of Second Phases during Solution Treatment of An Al-Zn-Mg-Cu Alloy Containing High Zinc. *Rare Met.* **2018**, *5*, 1–5. [[CrossRef](#)]
25. Peng, G.; Chen, K.; Chen, S.; Fang, H. Evolution of The Second Phase Particles during The Heating-Up Process of Solution Treatment of Al–Zn–Mg–Cu Alloy. *Mater. Sci. Eng. A* **2015**, *641*, 237–241. [[CrossRef](#)]
26. Mondal, C.; Mukhopadhyay, A.K. On the nature of T (Al<sub>2</sub>Mg<sub>3</sub>Zn<sub>3</sub>) and S (Al<sub>2</sub>CuMg) phases present in as-cast and annealed 7055 aluminum alloy. *Mater. Sci. Eng. A* **2005**, *391*, 367–376. [[CrossRef](#)]
27. Liu, J.; Li, H.; Li, D.; Wu, Y. Application of novel physical picture based on artificial neural networks to predict microstructure evolution of Al–Zn–Mg–Cu alloy during solid solution process. *Trans. Nonferrous Met. Soc. China* **2015**, *25*, 944–953. [[CrossRef](#)]
28. Deng, Y.L.; Wan, L.; Zhang, Y.; Zhang, X.M. Evolution of microstructures and textures of 7050 Al alloy hot-rolled plate during staged solution heat-treatments. *J. Alloys Compd.* **2010**, *498*, 88–94. [[CrossRef](#)]
29. Zou, X.L.; Yan, H.; Chen, X.H. Evolution of second phases and mechanical properties of 7075 Al alloy processed by solution heat treatment. *Trans. Nonferrous Met. Soc. China* **2017**, *27*, 2146–2155. [[CrossRef](#)]
30. Roknia, M.R.; Zarei-Hanzakia, A.; Abedib, H.R. Microstructure evolution and mechanical properties of back extruded 7075 aluminum alloy at elevated temperatures. *Mater. Sci. Eng. A* **2012**, *532*, 593–600. [[CrossRef](#)]
31. Papazian, J.M. Calorimetric Studies of Precipitation and Dissolution Kinetics in Aluminum Alloys 2219 and 7075. *Metall. Trans. A* **1982**, *13*, 761–769. [[CrossRef](#)]
32. Birbilis, N.; Cavanaugh, M.K.; Buchheit, R.G. Electrochemical behavior and localized corrosion associated with Al<sub>7</sub>Cu<sub>2</sub>Fe particles in aluminum alloy 7075-T651. *Corros. Sci.* **2006**, *48*, 4202–4215. [[CrossRef](#)]
33. Ma, K.; Wen, H.; Hu, T.; Topping, T.D.; Isheim, D.; Seidman, D.N.; Lavernia, E.J.; Schoenung, J.M. Mechanical behavior and strengthening mechanisms in ultrafine grain precipitation-strengthened aluminum alloy. *Acta Mater.* **2014**, *62*, 141–155. [[CrossRef](#)]
34. Booth-Morrison, C.; Dunand, D.C.; Seidman, D.N. Coarsening resistance at 400 °C of precipitation-strengthened Al–Zr–Sc–Er alloys. *Acta Mater.* **2011**, *59*, 7029–7042. [[CrossRef](#)]